Supplementary Information

Se vacancies-rich VSe_2 nanosheets with carbon-free for high-performance lithium storage

Qiwang Jiang,[a] Jie Wang,[a] Yan Jiang,[a] Long Li,[a] Xingzhong Cao,*[,b] and Minhua Cao*[,a]

[a]Key Laboratory of Cluster Science, Ministry of Education of China, School of Chemistry and Chemical Engineering, Beijing Institute of Technology, Beijing 100081, P. R. China.

[b]Institute of High Energy Physics, Chinese Academy of Sciences Yuquan St. 19, Beijing 100049, P. R. China.

E-mail: caomh@bit.edu.cn

Materials characterizations: The obtained products were characterized on a powder X–ray diffraction (XRD) (Bruker D8 X–ray power diffractometer) operated at 40 kV voltage and 50 mA current. XRD pattern was recorded from 10^o to 80^o (2θ) with a scanning step of 10^o/min. The morphologies of the products were examined by field emission scanning electron microscopy (FESEM, HITACHI S-4800) and transmission electron microscopy (TEM, JEOL JEM-2010). The Brunauer-Emmett-Teller (BET) specific surface areas of typical products were performed at 77 K in a Belsorp-max surface area detecting instrument. Raman spectra were recorded at Renishaw Invia Raman spectrometer, using an excitation laser of 633 nm. The photoluminescence (PL) spectra were obtained by using a Cary Eclipe florescence spectrometer (Varian, USA) with Xe lamp as the excitation source. Positron annihilation lifetime spectroscopy (PALS) was performed by a conventional fast-low coincidence spectroscope. The time resolution was 195 ps at room temperature, and 16 μCi ^{22}Na was used as the positron source. The X-ray absorption near edge structure (XANES) measurements were undertaken at Beamlines 1W1B at Beijing Synchrotron Radiation Facility (BSRF) using transmission and fluorescence modes.

Electrochemical measurements: The electrochemical tests were performed at room temperature by using coin cells (CR2025) on LAND CT2001A with a cutoff voltage of 0.01–3.00 V vs. Li^+/Li. The samples obtained above were used as active materials. For the anode preparation, the active material, conductive carbon black, and sodium carboxymethyl cellulose (CMC) with a mass ratio of 70:20:10 were mixed and ground

in a mortar. Deionized water was used as the solvent to make homogeneous slurry. The as-resultant slurry was uniformly pasted on a Cu foil and dried at 120 ^{o}C for 24 h in a vacuum oven. The cell assembly was performed in an Ar-filled glove box. The loading of the active material was about 0.8 mg cm^{-2}. The used electrolyte was 1 M $LiPF_6$ dissolved in an mixture of ethylene carbonate (EC)/dimethyl carbonate (DMC)/diethyl carbonate (DEC) (1:1:1, in vol%). A lithium foil was used as counter electrode. Cyclic voltammetry (CV) was measured by a CHI-760E electrochemical workstation with a scan rate of 0.1 mV s^{-1}. The impendence spectra were obtained by applying a sine wave with amplitude of 5 mV over the frequency range from 100 kHz to 0.01 Hz. To collect the active materials after cycling for the measurements of XRD, the electrodes were disassembled from the cells in an Ar-filled glove box, and then rinsed with absolute alcohol and DMC (Sigma-Aldrich, 99%) to remove the residual electrolyte.

Calculations of the capacitive contribution and diffusion-limited contribution: To quantitatively distinguish the capacitive and diffusion-controlled contributions to current, CV curves at a series of sweep rates were tested. Generally, the relationship between the measured peak current (i) and sweep rate (v) in a CV scan follows the following formula:

$$i = av^b$$

$$\text{then, } \log(i) = \log(a) + b \bullet \log(v)$$

Apparently, the b value can be obtained by fitting slope of the log(i) versus log(v) profile. When the b value is 0.5, it demonstrates a diffusion-controlled behavior, while

the b value of 1.0 corresponds to a capacitive behavior. The capacitive contribution and diffusion-controlled contribution can be further quantitatively distinguished assuming that the current (i) is a combination of the capacitor-like and diffusion-controlled processes according to:

$$i = k_1 v + k_2 v^{1/2}$$

We can calculate the capacitive and diffusion limited contributions by determining k_1.

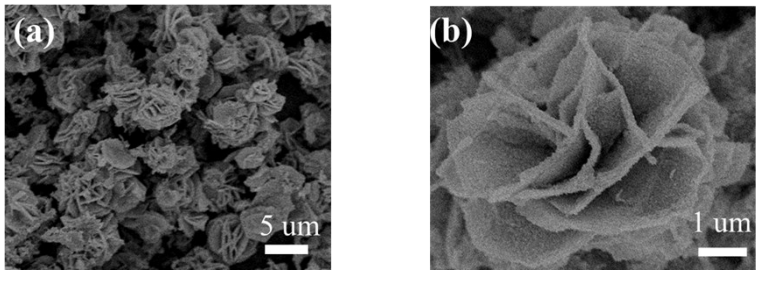

Fig. S1 (a) Low-magnification and (b) high-magnification SEM images of VSe_2-NSs.

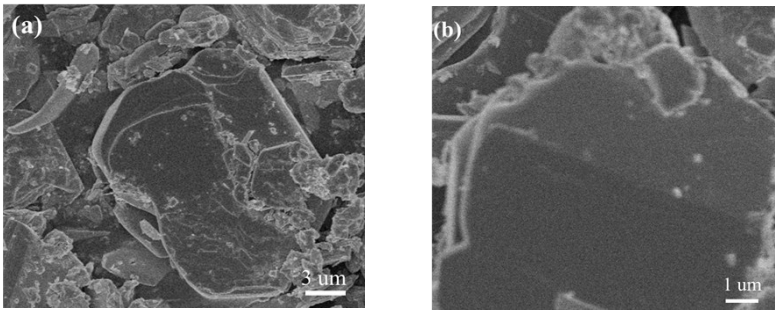

Fig. S2 (a) Low-magnification and (b) high-magnification SEM images of bulk VSe_2.

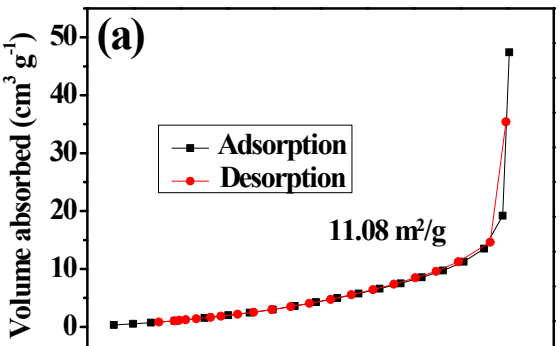

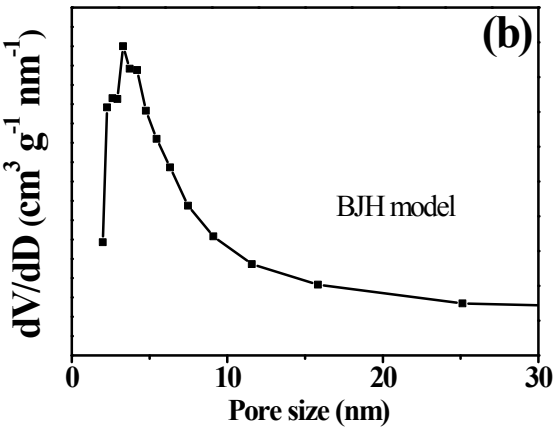

Fig. S3 (a) N_2 adsorption-desorption isotherms and (b) corresponding pore size distribution of bulk VSe_2.

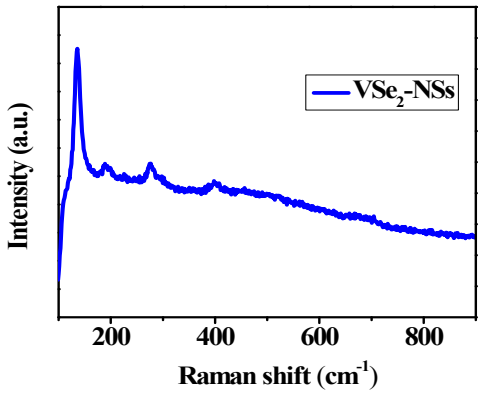

Fig. S4 Raman spectrum of VSe_2-NSs.

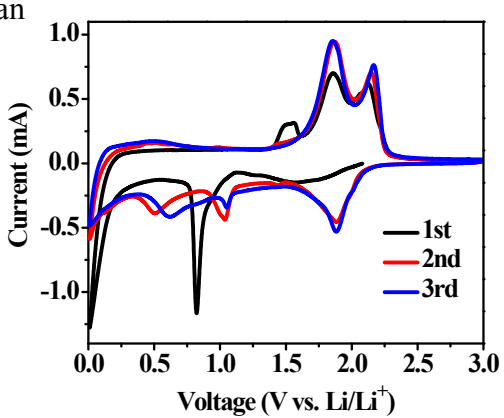

Fig. S5 CV curves of the bulk VSe_2 for the first three cycles at a scan rate of 0.1 mV s^{-1}.

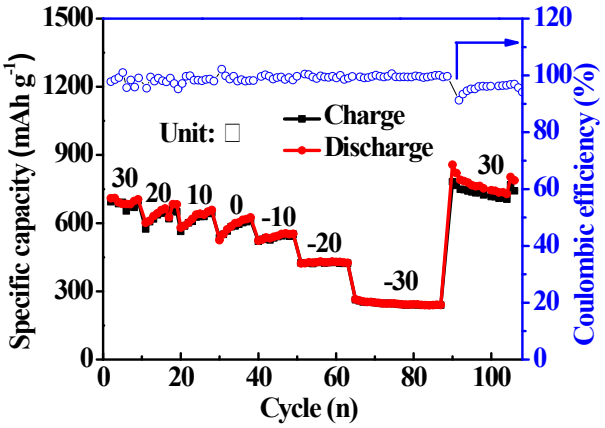

Fig. S6 Cycle performance of VSe_2-NSs at various temperatures at 0.1 A g^{-1}.

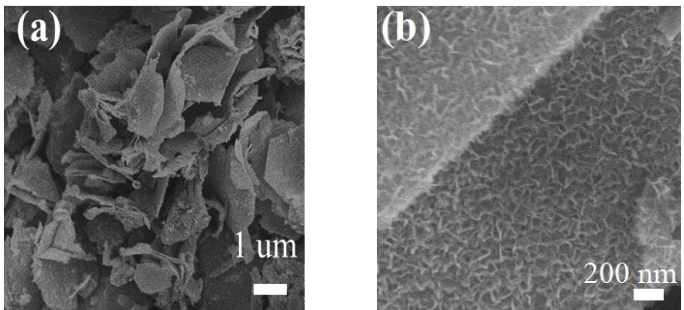

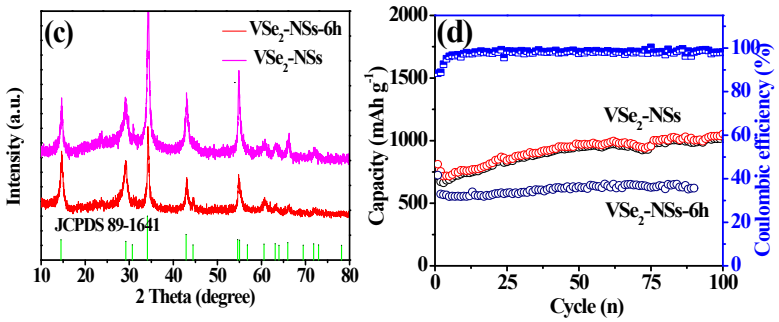

Fig. S7 (a,b) SEM images of VSe_2-NSs-6h. (c) XRD pattern of VSe_2-NSs-6h and VSe_2-NSs. (d) Cycling performance of VSe_2-NSs-6h and VSe_2-NSs at 0.1 A g^{-1}.

Table S1. Positron lifetimes and relative intensities of VSe_2-NSs -6h and VSe_2-NSs.

Samples	τ_1 (ps)	I_1 (%)	τ_2 (ps)	I_2 (%)	τ_3 (ns)	I_3 (%)
VSe_2-NSs-6h	**164.7 ± 5.2**	**37.3 ± 1.5**	**332.6 ± 3.9**	**60.8 ± 1.5**	**2.197± 0.047**	**1.895 ± 0.069**
VSe_2-NSs	**181.2 ± 4.4**	**59.4 ± 1.3**	**357.5 ± 3.1**	**38.7 ± 1.2**	**2.289 ± 0.044**	**1.871 ± 0.062**

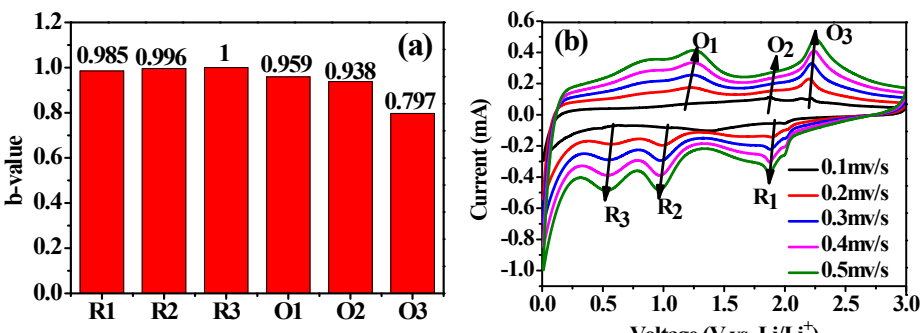

Fig. S8 (a) The b-values of different redox peaks. (b) CV curves of VSe_2-NSs at different scan rates.